Numerical Study of Friction-induced Pad-mode Instability in Disc Brake Squeal

S. Oberst*, J.C.S. Lai

Acoustics & Vibration Unit,
School Engineering and Information Technology,
The University of New South Wales, Australian Defence Force Academy,
Canberra, ACT 2600, Australia

PACS: 5011ss

ABSTRACT

Disc brake squeal as a major source of customer dissatisfaction is known to be friction-induced due to the highly non-linear contact of the surfaces between the disc and the pads. Brake squeal remains fugitive and difficult to predict also to some of its squeal frequencies have varying character and cannot always be associated with component modes. By means of structural finite element analysis, a simplified brake system in the form of a pin-on-disc is firstly approximated by a block sliding on a plate. By varying pressure and the friction coefficient, no mode coupling instability is observed and the mechanism extracted is purely of friction-induced nature. Especially in-plane pad motion in direction of and perpendicular to the sliding direction seem to feed-in most of the energy. These modes and their variability due to pressure variation, changes of lining material's elastic components and increased friction coefficient are studied in the following by means of the plate model. Then, it is shown, that these pad modes also exist for a pad-on-disc model with isotropic lining material. A second pad-on-plate model with more realistic lining material is developed which considers changes of elastic constants due to pressure variations. It is found, that changes in elastic properties of the lining material influence significantly the vibrations of the pad modes. The kinetic energy spectrum lifts up with changing pressure and stiffness and that combined effects of pressure synchronised with changing material properties are more severe than could be assumed by the complex eigenvalue method alone. By means of inverse Fourier transform of the response spectrum and non-linear time series analysis it is possible to detect the instability of the pad-on-plate model. The results show that friction-induced instabilities result from non-binding forces between pad and disc, with energy transfer from pad to disc causing dynamic instability, might trigger mode coupling or amplify underlying unstable modes predicted by the complex eigenvalue method. It is shown that these instabilities are most likely responsible for squeal frequencies occurring at frequencies far from the frequencies of the rotor modes, as often observed in brake squeal.

INTRODUCTION

Since the early 1930*s*, brake squeal has remained a research topic of high importance to brake systems' manufacturers and the automotive industry [1] due to customer complaints and their accompanying warranty costs. The high-pitched tonal character of most brake noise is annoying and has become more dominant due to major reductions in interior vehicle noise. Mechanisms thought to be responsible for brake squeal include stick-slip [2–4], negative gradient relationship between kinetic friction coefficient and sliding speed [5], sprag-slip [6], mode coupling or binary flutter [7], hammering [8], parametric resonances [9, 10] and moving loads [11]. Other mechanisms mentioned include thermo-elastic instability (TEI) [12, 13], stick-slip-separation waves [14, 15] and [16], and viscous instability [17]. All these theories have been comprehensively reviewed by Kinkaid et al. [18]. Other comprehensive reviews are those published by Akay [19] in which a general outline of the acoustics of friction is given, and Ouyang et al.[20] who focusses on the numerical analysis of brake squeal noise.

Brake squeal is fugitive and difficult to predict [21] and some of its squeal frequencies cannot always be associated with component modes. It has been shown that chaotic behaviour might develop in disc brake squeal, and a route to chaos has been demonstrated by means of non-linear time series analysis (NTSA) and cross- recurrence quantification analysis [22]. A correlation of the Complex Eigenvalue Analysis (CEA) and analysis in the time domain has been examined by [23] using an $3dof$ analytical model. If one or two modes are predicted by the CEA as unstable, the system anal-ysed in the time domain might have already shown three or more instabilities which are due to either quasi-periodic or chaotic behaviour. Hence, the CEA underestimates frequencies involved and in a chaotic regime, unstable behaviour cannot be determined by relying on only the unstable modes predicted by the CEA. For this purpose, the time trace has to be analysed by means of NTSA. On the other hand, it is well known that in numerical simulations the CEA often shows too many frequencies, which, if compared with measurements are not recorded on dynamometer tests as squeals [24–26]. As a consequence and due to the many mechanisms involved, it seems obvious that the analysis of brake squeal propensity in practice needs to be complemented by other analysis techniques in order to detect instabilities not due to mode coupling. In order to enhance prediction quality, the CEA in the frequency domain needs to be more oriented on the transient nature of brake squeal which can only be captured by a time domain analysis of a brake system [27]. Felske et al. [28] note, that not all squeal develops at, or even close to, the frequency of a brake component's normal modes. Murakami et al. [29] states that closeness to a component mode's frequency is not even a necessary condition for squeal. This indicates that either different mechanisms act exclusively on a specific brake system or that, for certain parameter combinations, mode coupling acts simultaneously or in a specific sequence with another mechanism (hierarchical). This means, squeal might only be audible, if for instance mode coupling is present but amplified by another mechanism or that mode coupling instability results after an initiating dynamic instability. Chen [1] shows that in an experiment with a steel pin on a plate, squeal noise is not a result of mode coupling instability. The squeal is described as *instanta-*

neous mode squeal where the squealing frequency is not coincident with the plate's frequency but 200 to 600Hz lower depending on the pressure and sliding velocity applied. Chen et al. [30] studied friction processes and in-plane modes. Assuming non-linearity to be the reason, often the squeal frequency decreased and was below the out-of-plane rotor frequency. Their recorded squeal signals show that either all the out-of-plane modes or only some frequencies which can be assigned to out-of-plane modes are visible; sometimes in only the low-frequency, but sometimes in the high-frequency, range, peaks appear. This could happen for either the transverse or the in-plane modes. However, the reason why sometimes only a few peaks appear, but not necessarily at the expected positions of the system modes, was not further investigated. In [31] the frequency response of pad modes under increasing pressure attenuated and it was further hypothesised that "the moment vibration of [the] pad can stimulate both rotor in- and out-of-plane vibration". Squeal not due to mode coupling was also observed by Ichiba et
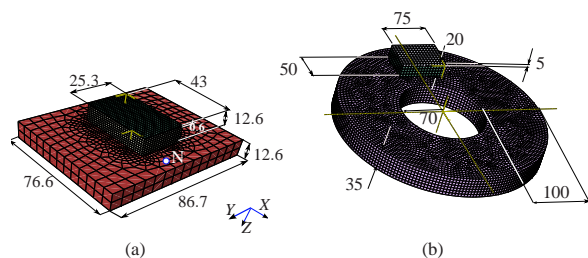

Figure 1: (colour online) (a) anisotropic pad-on-plate (model II) and (b) anisotropic pad-on-disc (model IV); *N* is measurement point to obtain a transfer mobility

al. [32] in experiments, occurring at 200 to 400Hz below the closest rotor's component frequency. The nature of the squeal was investigated by measuring the back-plate motion which showed no bending behaviour, moving almost *in-plane*. By studying the pad's tangential motion, it has been found that the variation of the friction force with time depends directly on the change in the lining's Young's modulus due to its compressibility which lead to squeal around 6kHz. The dynamic friction forces "do not bind" with the rotor: Fluctuations in friction force due to variations of lining thickness and Young's modulus were considered to be responsible for generation of feed-back vibrations. The squeal's neighbouring frequencies, belonging to components of the brake system, were sufficiently spaced and mode-coupling instability could be excluded. It is well-known, that pad-modes and their frictional contact play a major role in initiating instability. For example, Ouyang et al. [33] studied analytically friction-induced vibrations of an elastic slider on a disc for the stick-slip mechanism. By using phase-space plots of the slider's in-plane vibration and the disc's out-of-plane vibration, it was found that the transverse disc vibrations couple with the pad due to *friction non-linearity* and that an in-plane spring-damper system on the pad might induce additional instabilities or newly developing parametric resonances or change existing resonances even when the friction coefficient was constant [10, 34]. A parametrical resonance is due to a time varying system parameter change, so that instability occurs at one of the system resonances and might act amplifying. Matsui et al. [35] found, that near the contact patch, the higher shear forces induce vibrations which amplify the underlying transverse modes in a feedback loop due to the change of friction, prior to the braking process (see also [36]). This feedback loops amplifies the underlying transverse vibration modes causing them, together with the system resonances, to squeal. On a global scale, stick-slip is not present when a sufficiently high relative velocity is assumed [37, 38]. At the contact patch, it has been observed that local sticking is still possible and is accompanied by lift-offs of the pad which lead to *stick-slip-separation* waves [14, 16]. The *apparent* friction coefficient can be lower than the given friction coefficient due to the development of slip waves and a given constant μ does not allow to conclude about the pad-modes' contribution to the stiffness matrix, the apparent μ is generally lower [15]: the

different stresses in the contact patch determine the friction coefficient and as it comes to local slipping (slip-waves), the constant global friction coefficient serves so-to-say as an upper bound only. In [39], contact surface waves are investigated for different pressures and sliding velocities. When the velocity is high but slowly increases, slip-separation waves dominate the self-exciting character of the friction system. For high pressures and a lower velocity of the disc, the phenomenon of stick-slip is dominant. It is noted that these phenomena occur even with a *constant friction coefficient* and mark a major difference between their numerical model of a block in contact with a hard surface which does take into account elasticity of the two bodies in contact and analytical models, which do not account for area contact and elasticity. Ostermeyer [40] investigated the surface structure of pads and discovered patches, which experience micro-vibrations, due to local sticking and slipping, growth and destruction processes. Even though, these processes seem to be stochastically distributed, they are able to synchronise resulting in macroscopic tangential vibrations. This synchronisation has been analysed with initially decoupled stick-slip oscillators. The multi-dof system resembles the cross-sectional boundary layer of a FE contact model where each element could stand for a separate oscillator, able to feed in energy. Due to this importance of pad vibrations, it has already been suggested that a CEA, as a function of a pad's modes, should be performed [37]. By means of a laboratory brake, it has been found that, with varying loads, a change in pad resonances of up to 25%, due to variations of the pad-disc's 'angle of attack' up to 15%, are possible. By considering changes in all the operating conditions of the experimental setup in the worst case scenario, it has been found that a maximum change in the pad's in-plane frequencies of 11.2kHz seems possible. It is difficult to capture the pad vibrations and their properties because lining material properties change with operating conditions.

One uncertainty accompanied with the pad is beside its friction contact with the disc its lining material model. It is known that brake squeal is sensitively dependent on the lining material's properties which change when different pressures are applied, [18, 41, 42]. However, often in numerical simulations and analytical models, the material property of the lining material is simplified as constant and orthotropic or even constant and isotropic. Brake lining material should be treated as a visco-elastic/plastic material with highly non-linear load, time and history dependencies [43]. A good summary of friction material's properties, and their changes due to temperature variations pressures is given in *Disc Brake Squeal* [41], (ch. 12). Friction material is described as a non-linear meso-scopic material with anisotropic characteristics. In Lou et al. [44], non-asbestos organic (NAO) lining materials are described as (1) inhomogeneous and anisotropic, and (2) highly non-linear with respect to loading. Changes in its properties have mostly been studied experimentally but have not, as yet, been related to brake squeal. One problem is that properties of brake lining material are difficult and time-consuming to measure. Brecht et al. [45] described the lining's elastic properties as being similar to those of a spring which dissipates energy via a viscous flow. Based on that, a material model is developed and for proper modelling of brake lining, an orthotropic visco-elastic material is suggested.. Wegmann et al. [46] define the pad's compressibility as combined physical effects which relate the elastic and plastic deformations of the lining material, after a series of load cycles, to each other. Compressibility is not a friction material-specific characteristic but, describes a property of the whole pad assembly: dependent on its material composition, different layers (sandwich structure) and geometry (form factor). The variability of a pad's lining compressibility due to manufacturing tolerances is another problem encountered in terms of changes in the material properties of a brake system under operating conditions [47]; that is, the material matrix entries change during operation but the changes are different for each batch of lining material due, for instance, to changing degrees of inhomogeneity. Sanders et al. [48] studied *cyclic* compressibility as a function of the preload, temperature and velocity of a semi-metallic brake lining material by means of a full factorial design analysis. Increasing the temperature

from 20 to 300°C or lowering the preload from 8 to 4kN halved the compressibility. Decreasing the frequency (which was equated with rotational velocity) from 20Hz to 1Hz reduced compressibility by 10% which is almost its increase in stiffness. Compressibility can be related to stiffness and it was found that doubling the preload increases the stiffness by 100%, but that halving the compressibility due to increased temperature leads to a 50% reduction in the stiffness of the elastic constants. It has to be noted that these changes occurred at rather low pressures of up to 60kN. Yuhas et al. [43] studied three pad compositions' anisotropic lining materials (engineering constants) by measuring the spatial variations of ultrasonic attenuation, using static pressures from 0.5 to 8.0MPa. It was observed that the elastic constants vary highly non-linearly with changing pressure, especially in the low pressure range. The "through-thickness" component (derived from the out-of-plane velocity), C_{33}, varies by up to 60% and, in total, the magnitudes of the elastic properties vary by 10% for the three lining compositions investigated.

In this paper, in-plane modes of the pad are investigated for their role in friction-induced squeal and triggering mechanism and in amplifying mode-coupling instability. In the first part of the paper, pad-modes obtained using complex eigenvalue analysis for a pad-on-plate system are investigated and a link to experiments reported by Chen [1] is established. Then a simplified brake system in the form of pad-on-disc is considered with non-linear pressure dependent lining material properties. In the second part, the kinetic energy for plate and disc models is studied in order to establish the kinetic energy, to predict instability based on the behaviour of pad modes. In the last part, by applying inverse Fourier transform to the forced response of the pad-on-disc system, non-linear time series analysis tools are used to investigate dynamic invariants of the pad-on-plate system.

NUMERICAL MODELS

In this paper, four different models (I-IV) based on iso- and anisotropic (transversely isotropic) material properties and two model types are used, *plate* and *discs*: isotropic pad-on-plate model (I), an-isotropic pad-on-plate model (II), isotropic pad-on-disc model (III) and an-isotropic pad-on-disc model (IV), as shown in Figure 1. *Plate* models represent a slider on a moving plate, similar to the analytical models used in [49, 22] but with elasticity and area contact. These models represent a simplified annular disc 'cut open' and stretched to a plate shape [50–53]. As previous simplified brake systems were designed primarily to display mode-coupling instability due to split modes merging together (*mode merging* [54, 55]), this type of mode coupling instability is eliminated by using a plate model.

For the pad, the form factor, (that is its size, geometrical features) remains the same for isotropic and anisotropic pad-on-plate/disc models except that, for the anisotropic pad, a back-plate is attached to the lining material causing higher out-of-plane stiffness. For the pad-on-disc model (III), the isotropic material properties are modally updated via the finite element method (FEM) to closely match the three plates bending modes - 5.7, 8.2 and 11kHz identified in [1]. For the elastic modulus and the Poisson's ratio, 210GPa and 0.305 are used, the density is calculated from the weights of the pin (110g) and the plate (648g) as $8025/7744 \text{kg/m}^3$. Thus, under free-free boundary conditions, the *pad*-modes were found at $(p,q) = (1,0) = 5774.8 \text{Hz}$, $(0,2) = 8083.3 \text{Hz}$ and $(2,0) = 11044 \text{Hz}$, where p and r are the nodal lines in the longitudinal and transverse in-plane directions, respectively [56]. The nomenclature of the disc follows that [57], where (m,n,l,q) represents out-of-plane m nodal circles and n nodal diameters, in-plane p nodal circles and q nodal radial lines. For example, if $n = 3$ then $(0,3,0,0)$ describes a disc mode with three nodal diameters; If this mode becomes unstable, it is referred to as $(0,3\pm,0,0)$-mode with $\pm$ indicating a positive $(+)$ and a negative $(-)$ travelling wave.

In order to investigate the influence of material property changes of the brake lining in model IV, data taken from Yuhas et al. [43] are given in Figure 2 for 4 different pressures: 0.5, 2.5, 5 and 8 MPa. The shear moduli were estimated with a 10% change at each pressure value [43]. For the other models, only either a pressure or material variation was performed. Numerical simulations are based on ABAQUS 6.8-4 using *finite sliding*, the *kinematic constraint* contact algorithm with a *constant* friction coefficient. A mesh-independence study was performed, as recommended in [58]. The meshes used here give a difference in the estimate of frequency of less than 1% when the number of elements is increased by $\approx 298\%$. Table 1 shows the number of each specific element type, the numbers of elements in the FEM. Only *incompatible modes*' elements ($C3D8I$) are used in order to achieve improved bending [59] and convergent behaviour [58]. The properties of the lining materials of models II and IV are taken from Yuhas et al. [43] and are given in Table 1 for a pressure of $0.5MPa$. For models I and III standard properties of isotropic cast iron and steel are used.

DYNAMIC BEHAVIOUR OF PAD MODES

Problem Scope

Emphasis in this study is on models I and IV (Figure 3), as model I simulates an experiment performed by Chen [1] and model IV provides the opportunity to investigate the influence of changes in the lining material properties due to its compressibility under load for a simplified brake system (pad-on-disc) also used in [50, 51, 53]. The models studied focus on the influence of (a) geometry: plate model I $\rightarrow$ disc model III and (b) material properties: isotropic disc model III $\rightarrow$ anisotropic disc model IV. In this study, the friction coefficient and the pressure are varied in order to simulate the braking process in the frequency domain. Hereby, it is important to keep in mind, that even though a constant friction coefficient is applied, implicitly a negative friction/velocity gradient is assumed by increasing the friction coefficient. Thereby, the velocity is assumed to be nearly constant during braking. Figures 3(a) and (b) depict two
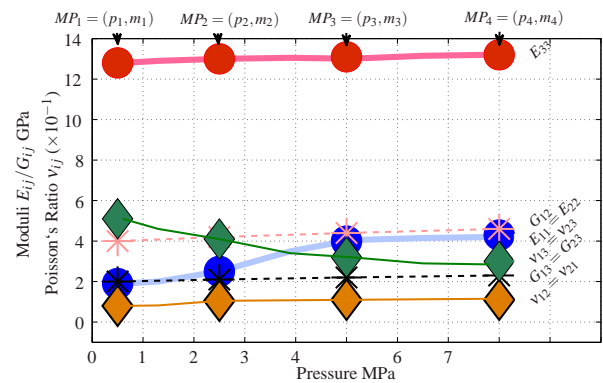

Figure 2: (colour online) Material properties of measurements taken from Yuhas et al. [43]; MP_1-MP_4 indicate material points

modes which indicate the motions of the (isotropic) steel pad. The pad's dominant movements are indicated by double arrows. Figure 3(c)-(d) depict the pad-on-disc model (IV) with the combined effects of pressure, friction and disc rotation. These effects give the pad a slight twist so that for normal modes, the tangential motion obtains a stronger radial component for complex modes, as can be seen in Figure 3(c). In comparison to Figures 3(a) and (b), deformations of the isotropic pad are rather limited whereas larger deflections can be visually observed for the transversely isotropic lining material, by applying identical scaling factors. For models I and II, pad vibrations in $x - /y-$ direction are observed (translational rocking motions): a pad oscillating in-plane perpendicular to its sliding direction (P_y) and one mode oscillating with the direction of relative velocity (P_x). For model I and II, a pad's in-plane mode, which rotates in-plane about its centre of gravity lies around 8.1kHz out-

side the frequency range of 2.5-6.5kHz. This kind of mode will be named rotational mode P_{rot} in the course of this study. The in-plane pad motion of the disc models always comprises three basic motions: (i) in-plane translational but perpendicular to the direction of the disc's motion (radial mode P_r); (ii) also translational but in the direction of the disc's motion (tangential mode P_t); and (iii) rotational in the third pad mode (rotational mode P_{rot}). Unless otherwise mentioned, the friction coefficient μ is increased in 0.05 steps, from 0.05-0.65. Pressure on the pad is uniformly distributed and takes values in the range of $0.001, 0.5, 2.5, 5.0, 8.0$MPa. Depending on (a) chosen boundary conditions constraining the pad, (b) mesh refinement and lining material properties, (c) applied pressure, (d) changes in lining material stiffness and (e) alteration of the friction coefficient μ, both the frequencies and amplitude of vibration change. Altering the boundary conditions to more node constraints (e.g., line or area constraints) has the effect of moving the pad modes to higher frequencies. With more nodes constraint (e.g. an area constraint on each side), the pad modes come to lie around $15kHz$ which is still in the audible range. For a real brake system, the fixation of the pads is limited to relatively small parts of the *pad ears* which are connected to springs (abutment clips) and consist of only two line contacts each, resembling the contact of the abutment clip. It is assumed that these springs are less rigid than the boundary conditions applied here. At the beginning of this

Table 1: Material parameters for models I-IV

	Models/ No. Elements	Material Constant	Plate/Disc	Lining	Backplate
isotropic	**I**/6,312 **III**/26,153	E GPa ν ρ kg/m³	210/110 0.305/0.28 7744/7100	180/210 0.3/0.3 8025/7200	–– –– ––
anisotropic	**II**/ 6,312 **IV**/ 31,355	E_{ij}GPa ν ρ kg/m³	146/146 0.29/0.29 7100/7100	see Table 2	207 7860

study, the sensitivity of the lining material properties to changes in the friction coefficient and the elastic constants of the lining for the pad-on-plate only, was briefly investigated in order to check if a more realistic lining material (model II) would (i) exhibit the number and kind of modes and (ii) have similar sensitivity to stiffness changes as a steel pad (model I) rubbing on a plate. The purpose of this preliminary computational experiment is to gain a feel for the importance of the material properties relative to changes in the friction coefficient for the isotropic and anisotropic lining material. Isotropic steel and the transversely isotropic (in-plane differ from out-of-plane components) pad components, E_{ii}, G_{ij}, ν_{ij} with $(i, j \in x, y, z)$, were altered by increasing and decreasing the elastic constants by 2.44%. For the transversely isotropic lining material these changes are assumed to result from increased brakeline pressure. As steel itself is not very pressure-dependent, these 2.44% represent realistic changes in the steel lining (pin material) only if it is assumed that the temperature increases or decreases.

Table 2: An-isotropic lining material properties according to Figure 2 dependent on pressure [43] for models *II* and *IV*

Pressure MPa Constant	p_0 10^{-3}	p_1 0.5	p_2 2.5	p_3 5.0	p_4 8.0
E_{33}GPa	1.9	1.9	2.5	4.0	4.3
$E_{22} = E_{11}$GPa	12.8	12.8	13.0	13.1	13.2
G_{12}GPa	2.0	2.0	2.1	2.2	2.3
$G_{13} = G_{23}$GPa	4.0	4.0	4.2	4.4	4.6
$\nu_{23} = \nu_{13}$	0.51	0.51	0.41	0.32	0.30
$\nu_{32} = \nu_{31}$	0.08	0.08	0.105	0.11	0.115
$\nu_{12} = \nu_{21}$	0.08	0.08	0.105	0.11	0.115
ρkg/m³	2500	2500	2500	2500	2500

Three temperatures, $\{0, 22, 44\}°$C were used to vary the stiffness of the isotropic lining material. An estimation of the temperature-modified Young's modulus is calculated from $E_t = E \left(a - \frac{(t-b)^n}{C} \right)$,
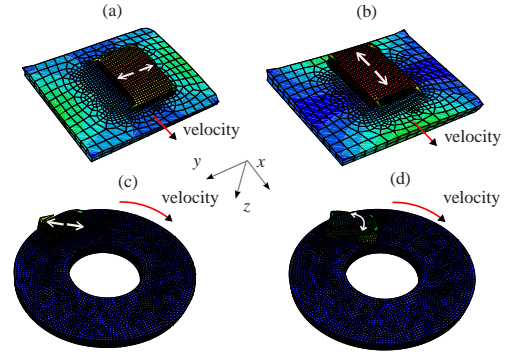
Figure 3: Isotropic pad-on-plate model (I): oscillations in (a) $y-$direction (mode P_y) and in (b) $x-$direction (mode P_x); Anisotropic pad-on-disc model (IV): (c) dominant motion of tangential mode P_t and (d) rotational motion of mode P_{rot}.

and $a = 1, b = 22°$C, $n = 1, E_n = E = 180$GPa and $c = 900°$C [60]. The results for the first 6 of 7 modes calculated by CEA in the frequency range of 1-7000Hz are depicted in Figure 4 ($p = 1$kPa, $\mu \in \{0.05, 0.5, 0.75\}$, $v = 1$m/s). Non of these modes is predicted to be unstable. For the pad-on-plate model, the first three modes and the 6th mode were dominated by the plate movement but then for 4th and 5th mode, the pad's movement became dominant.
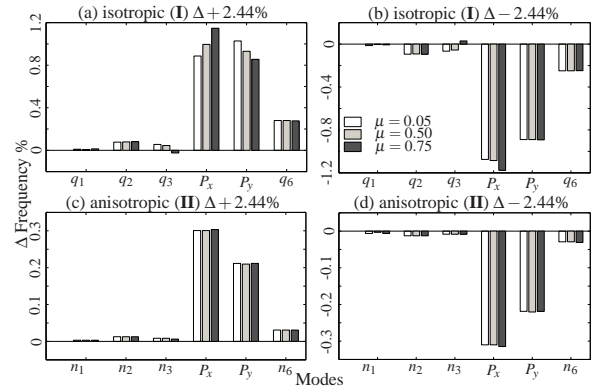
Figure 4: Effect of changing (Δ) Young's modulus and Poisson's ratio of isotropic and anisotropic pad-on-plate model (I) to stiffer (a+c) and more compliant (b+d) values; for model II trend of change taken from Figure 2

The pad modes are acting almost as in-plane rigid body modes. Due to this in-plane vibration especially in x-direction (tangential direction) a lot of energy can be fed-in into the system[61] which might result in destabilisation. The pad modes for the an-isotropic pad-on-plate model (II) are of the same kind than those of model I. In summary, four observations can be made: (1) The sensitivities of the frequencies of pad modes to changes in stiffness of the lining materials are smaller than that of the steel pad, being, at most, a change of $\pm 1.2\%$ (model I) and $\pm 0.3\%$ (model II) for a $\pm 2.44\%$ change in the elastic constants. Even though these changes do not seem large, it should be noted that for model I, the assumed maximum temperature was only $44°$C whereas the brake system's components are designed to be mechanically stable at temperatures up to $650°$C [62]. Also, for model II, as lining materials can change their stiffness by more than 100% [45], the 2.44% taken here is a rather conservative value. (2) Changes in frequency due to only changes in the friction coefficient from $0.05, 0.50$ to 0.75 (at a relatively low pressure of 10^{-3}MPa) are, at most, about 0.2%. (3) The 4th and 5th pad modes in which the pad is moving in a dominantly rocking motion (x, y-direction) are the most sensitive to changes in the lining's stiffness. (4) Due to the boundary conditions and the coupling of the pad and plate, there are 7 *system modes* compared with 5 component modes

of the plate in the frequency range investigated. As a final interesting outcome, the frequencies of the system modes depicted in Figure 4 are within 6% of the frequencies reported in the experiment by Chen [1].

Dynamic Behaviour by means of CEA

In the following section, changes in the complex eigenvalues of the pad-on-plate model I (Table 1) are investigated. The material properties for the isotropic pad-on-disc model (III) remained constant but the pressure was varied from 10^{-3} MPa to 8.0 MPa. The friction coefficient μ altered in 0.05 steps from 0.05 to 0.65 and a velocity of $v = 1$ m/s ≈ 3.6 km/h. Apart from frictional damping, no other dissipation mechanism was active. In Figure 5, the variation

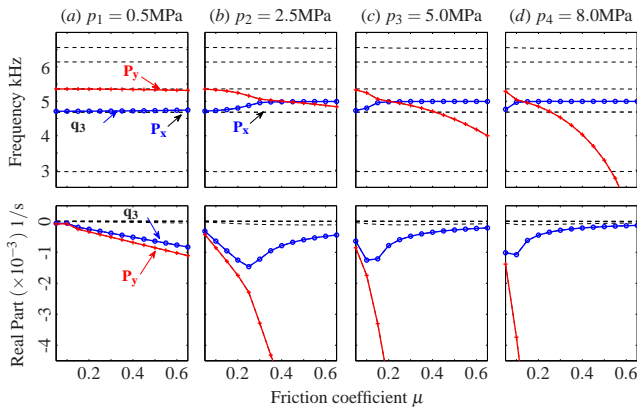Figure 5: (colour online) Pressure variations on isotropic pad-on-plate model (I): (a) $p_1 = 0.5$ MPa; (b) $p_2 = 2.5$ MPa; (c) $p_3 = 5.0$ MPa; and (d) $p_4 = 8.0$ MPa.

of frequencies and real parts (representing damping) of the complex eigenvalues of system's modes with pressure are depicted. Pad modes P_x and P_y remain stable and are indicated by thicker lines as well as the 3rd mode. The results for 1kPa are not presented as they look qualitatively like the results for 0.5MPa except that the real parts are decreasing slower with increasing friction coefficient. By increasing the pressure and the friction coefficient, the following observations can be made:

(1) in the frequency range investigated, the CEA does not detect an instability;

(2) the pad mode perpendicular to the sliding direction P_y decreases and the 3rd mode, with a strong component in of the pad in $x-$ direction increases in frequency;

(3) changes in the frequencies of P_y and q_3 are more pronounced when the pressure increases and a $s-$shaped curve (frequency over μ) moves in the direction of the lower friction coefficients (see Figure 5 (a)-(d)); and

(4) the eigenvalue's real part shows an almost linear decay with increasing friction coefficient and, after reaching a minimum, exhibits approximately square-root increasing behaviour.

(5) q_3 is strongly influenced by the pad motion as it lies close to the pad mode $q_4 = P_y$.

It has to be noted that, for P_y, the complex eigenvalue's real part takes very negative values which probably indicates that the vibration in this direction becomes greatly suppressed by increasing pressure. In experiments of a similar system [1], mode-coupling type instability was excluded due to the slider not having flexible modes in the frequency range investigated. By investigating the pad-on-plate model using CEA, no instability due to mode coupling could be observed for a sliding velocity of 1m/s. The most interesting point is that, although it could be confirmed that instability was not detected by the CEA. Also, increasing the complex modes extraction up a frequency range of 25kHz, does also not show any instability. However, the pad modes excite the *"still flexible vibration"* [1] of

the plate and show large changes in frequency and real part. In the next step, the anisotropic pad-on-disc model IV is considered as a model of a simplified brake system. The structure changes in the following ways:

(a) rotation is applied to an annular disc thereby allowing for *mode-merging of the split modes*, as a specific kind of mode coupling [63, 55];

(b) mode P_x now corresponds to an in-plane tangential pad mode (P_t) and mode P_y to an in-plane radial pad mode (P_r) ;

(c) a rotational pad mode (P_{rot}), appears in a frequency range of 1Hz $- 7$kHz;

(d) the pad material changes from isotropic to an-isotropic;

(e) the velocity increases to 10rad/s ≈ 11.4km/h and

(f) the lining material is non-linearly dependent on the pressure (see Figure 2).

Case Study *Complex Eigenvalue Analysis* (Model IV)

In order to investigate the effects of changes in non-linear material properties on pad modes, cases A to C are examined (see also Figure 2).

(A): The pressure is left constant at a low value of 1kPa; variations concern only changes in the material properties $m_1 - m_4$.

(B): The pressure varies from 0.001 to 8.0MPa with the material properties kept constant at m_1

(C): The material properties for the four different pressures from 0.5 to 8.0MPa as given in Table 2 are used.

In all three cases, in a frequency range of 1Hz to 7kHz, only the disc's $(0, 3, 0, 0)$ split mode becomes unstable.

Case A   In Figure 6, the results of Case A are depicted. P_{rot}, P_t, P_r and $(0, 3\pm, 0, 0)$ are the rotational, tangential, radial pad and out-of-plane split modes of the disc, respectively. In Figure 6, the critical friction coefficient for bifurcation is marked by TP where the damping ratio $\zeta = -2\frac{\Re\{x\}}{|\Im\{x\}|} \geq -10^{-5}$. $\Re\{x\}$ and $\Im\{x\}$ denote the eigenvalue's real and imaginary parts, respectively. At low pressures, as solely frictional damping and variations of the lining material's elastic constants are applied, the complex eigenvalues' imaginary parts merge in a perfect manner: two modes transfer energy at exactly the same frequency and no corridor is visible between the two modes' freuquency, according to [17]. By stiffening the lining material, the transition point moves to higher friction coefficients. Assuming an increase in the friction coefficient for a decreasing velocity, this generally corresponds to predicted squeal at a lower relative velocity. Therefore, the complex eigenvalue's real part obtains absolutely lower values at higher friction coefficients. That the system does not behave more stably with a decreasing value of the positive eigenvalue's real part has been argued by Oberst and Lai [50] due to the acoustic power not increasing with increasing negative damping. Therefore, the term '*stabilising*' is avoided here when referring to an increasing value of the critical friction coefficient.

Case B   As shown in Figure 7, the material properties are kept constant at those of the material point, $MP_1 = (m_1, p_1)$ (Figure 2) but the pressure is varied from 0.5MPa to 8.0MPa. In Figure 7(a) to (d), the changes in frequency, especially of P_{rot} and P_r, become visible: the frequencies of the two pad modes P_t and P_r decrease with increasing pressure and friction coefficient. The radial and rotational pad modes (P_r and P_{rot}) decrease n frequency; however, even though a general trend can be perceived, the modes' frequency changes are visible and might be described as fluctuating. First of all, their frequencies are not only going down as the trend is sometimes broken due to these large changes in frequency, and secondly, due to an oscillating and uncertain friction coefficient in the time domain, large fluctuations are for sure. The change in frequency of mode P_t is negligible by comparison. Also, for 2.5MPa and 8.0MPa,

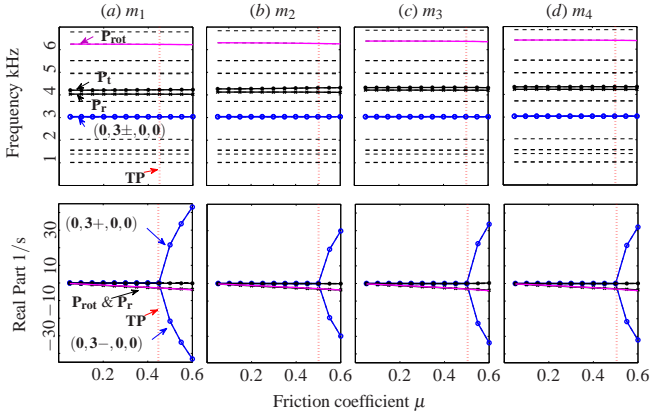the radial pad mode vanishes, and might act like a switching mecha-

Figure 6: (colour online) Case A: varying material properties (coordinate m_i in Figure 2) and a constant pressure of 1kPa. P_{rot}, P_t and P_r give the rotational, tangential and radial pad modes. $(0, 3\pm, 0, 0)$ is the disc-dominated transverse mode with 3 nodal diameters (positive $(+)$ and negative $(-)$ travelling wave). TP marks the transition point.

nism in terms of frequency in the time domain, as shown in Figures 7(b) and (d), when the friction coefficient exceeds $\mu = 0.55$ and $\mu = 0.40$, respectively. One interpretation is that, vibrations in the in-plane radial direction cease if both the pressure and friction coefficient are sufficiently high. It is interesting that in Figure 7 (d), indicated by a circle at $\mu = 0.65$, the radial mode (P_r) re-appears. Further, for 8.0MPa, the transition point changes from $\mu = 0.40$ to $\mu = 0.45$, thereby indicating possible squeal at a lower velocities . It can be seen from Figures 7 (a) to (d), that the real parts fo the complex eigenvalues decrease with increasing pressure and friction coefficients. The real parts of the rotational and radial pad modes are so small that they are only visible in Figure 7(a). The black lines in (b) and (c) give the real part of the tangential pad mode (P_t). The fluctuations in the modes' eigenvalue frequencies with the friction coefficient can be observed in the real parts of the complex eigenvalues for these modes perhaps because of different energy transfer between modes. It can be assumed that these frequency changes are due to energy being transferred differently between modes due to variations of the friction coefficient. As it can be seen in Figure 7 (a), the mode coupling of the split modes is imperfect because of the higher pressure value of Case B compared with that of Case A (Figure 6). By increasing the pressure, this imperfection is amplified (Figure 7 (a) to (d)). Apart from frictional damping, no other dissipation mechanism is present. In [17], by incorporating viscous damping, imperfect mode-merging resulted from *viscous instability* for a mode-coupling type instability. A similar effect can be observed here: for increasing pressure and frictional damping, the spectral characteristics change such that mode-merging is not perfect anymore.

Case C As shown in Figure 8, the pressure and material values are varied (Case C) according to the material points in Figure 2. Globally, similar behaviour as for Case B can be observed, except that the curves look smoother. Again, the frequencies of P_{rot} and P_r experience large changes and the unstable mode pair, $(0, 3\pm, 0, 0)$, splits imperfectly (Figure 8 (a) to (d)). However, probably due to the combined effects of increase in pressure and changes in material properties, the critical friction coefficient increases. It is interesting to note that the radial mode still vanishes, although at higher pressure values than for Case B, and does not reappear (see Figure 8 (d)). Similar to P_x of the isotropic pad-on-plate model, the tangential pad mode's (P_t) real part has a clear minimum. As in Case B, the change in spectral properties of the radial and rotational pad
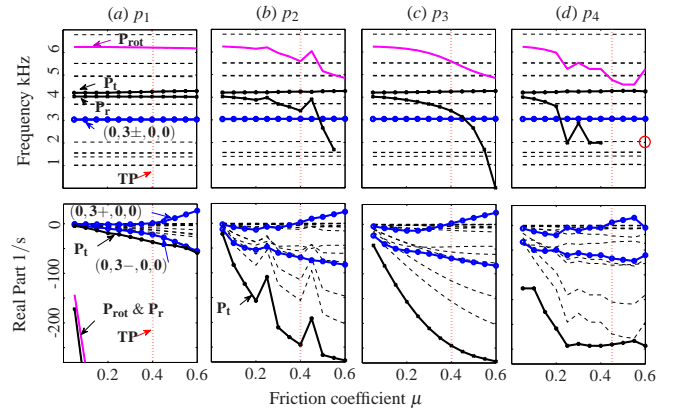

Figure 7: (colour online) Case B: constant material properties according to Figure 2 but varying pressure loads (L) of $p_1 = 0.5$MPa to $p_4 = 8.0$MPa. P_{rot}, P_t and P_r indicate the rotational, tangential and radial pad modes, respectively. $(0, 3\pm, 0, 0)$ is the disc-dominated transverse mode with 3 nodal diameters (positive $(+)$ and negative $(-)$ travelling wave). TP marks the transition point.

modes are the most severe. To analyse changes in the frequencies of the pad modes, especially of P_t, in more details, the sum of the modes standard deviation in frequency, $\bar{\sigma}$, estimated as a dispersion parameter of all the modes in a frequency range of 1Hz $- 7$kHz, for the four pressure cases is calculated and shown in Figure 9 (a) to (c). The modes for the an-isotropic pad-on-disc system are numbered $1 - 20$. For case A (Figure 9(a)), modes 12 (P_t) and 17 (P_{rot}), show a relatively large value of 35 and 40Hz, respectively. Here, especially for a pressure of 2.5MPa, the dispersions of P_t and P_{rot} are relatively high . Other modes which change their eigenfrequencies quite a lot are $7, 8$ and $11, 13$ which are predicted as unstable pair of the $(0, 3, 0, 0)$ mode, the radial pad mode (P_r) and the neighbouring $(0, 4-, 0, 0)$ mode, respectively. The minus of the $(0, 4-, 0, 0)$ mode indicates the split mode with a negative travelling wave relatively to the rotation direction. All other modes show negligible changes in their frequencies. In Figure 9(b), for Case B, by applying different pressures but leaving the material properties at the material point of MP_1, large changes for the P_r and P_{rot} pad modes can be observed. The sum of the standard deviations increase up to 1.5kHz and 0.5kHz (variation $p_4 = 8.$MPa), respectively. The sum of the standard deviations for all four pressure variations reaches a maximum of 3981Hz for P_r, 1650Hz for P_{rot} and 106Hz for P_t. The mode
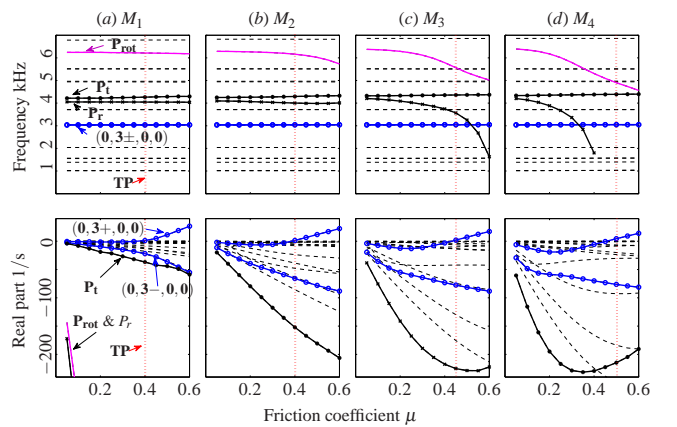

Figure 8: (colour online) Case C: varying material properties (M), and varying loads (L). P_{rot}, P_t and P_r stand for the rotational, tangential and radial pad modes. $(0, 3\pm, 0, 0)$ is the disc-dominated transverse mode with 3 nodal diameters (positive $(+)$ and negative $(-)$ travelling wave). TP marks the transition point.

P_r displays the highest standard deviation (1640Hz), followed by the rotational pad (P_{rot}) mode 17 with 1330Hz. However, the combination of the lining material stiffening and increased pressure results in more than a halving of the summed standard deviation, from around 3981Hz to 1640Hz, which may be interpreted as stabilising in terms of frequency variations. Then, in Figure 9 (d), the faned out standard deviation estimates of the second pad mode($\bar{\sigma}(P_t)$) is presented, for Cases A to C for variations in material, pressure and for the synchronised case C (pressure with material changes). Two basic findings are observed: (i) the sensitivity of mode P_t to higher pressures is lower than that of the P_r and P_{rot} modes; and (ii) the combined effects of load variation and non-linear material changes lead to an increased standard deviation which is still higher than that for disc's out-of-plane modes. This means that, for the pad mode P_t, the combined effects of load and alteration of material introduce more variability into the system.

Dynamic Behaviour in terms of Kinetic Energy

From results obtained by the CEA, noticeable changes in frequencies and the real parts of the complex eigenvalues are observed. The modal frequencies and real parts, due to changes in pressure, materials' elastic constants and friction coefficients are investigated for models I and IV. The complex eigenvalue method, based on the extraction of mode shapes, does not take into account the influence of other modes due to a structurally damped system under excitation. The change in frequencies is estimated based on mode shapes and is, therefore, linked to the modes sensitivity. The magnitude of a positive real part of the complex eigenvalue is in itself not a useful predictor for a non-linear system because it only predicts the linearised state, and mostly mode coupling is detected. Even the determination of the critical friction coefficient seems debatable [53].
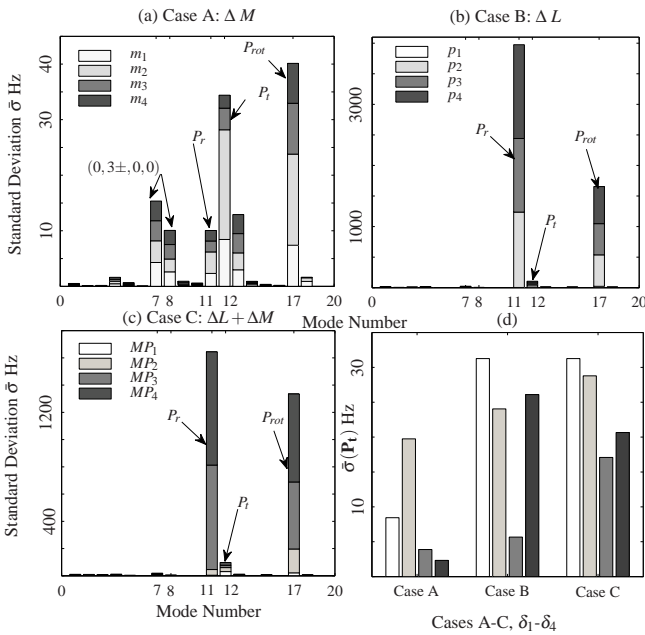
sity. As the V and ρ remain constant, the only change expected is the strength of the underlying velocity field. Figure 10(a) shows the effect of increasing the pressure on the kinetic energy of model I from 10^{-3} to 8.0MPa and for each pressure, the friction coefficients μ from 0.05 to 0.65. The peak frequencies f_1 to f_4 correspond to the 1st, $(2^{nd}, 3^{rd})$, $(4^{th}, 5^{th})$ and $(6^{th}, 7^{th})$ mode, see Figure 4. Some of the modes given in Figure 4 do not show visible frequencies in the energy spectrum as they are smeared and coupled with neighbouring frequencies due to their interactions and global structural damping of 0.4%. Additionally, the kinetic energy spectrum for the plate alone and for 10^{-3}MPa with $\mu = 0.01$ and $\mu = 0.001$ is plotted. The kinetic energy of the plate alone, does not show any peaks at frequencies greater than 3kHz, although plate modes are present over the frequency range investigated: at $3.04, 4.40, 4.44, 5.71$ and at 6.05kHz. The incorporation of the pad with pressure and a very low friction coefficient of $\mu = 0.001$, only moves the plate mode at around 3kHz down to 2.7kHz and no other modes are visible. However, with an increase of the friction coefficient up to $\mu = 0.01$ new peaks appear. Then, increasing the pressure increases the kinetic energy spectrum. A further effect of increasing the friction coefficient is to produce broader and higher peak amplitudes for most of the frequencies, with the exception of only the first frequency (f_1) which is dominated by a plate's bending mode with almost no pad movement involved. The kinetic energy spectrum shows the modes responsible for feeding in most of the energy. The feed-in energy can be estimated by means of *balance in energy*:

$$E_{kin} + E_{int} + E_{fric} - E_{for} - E_{visc} = const. \qquad (1)$$

$$\Longrightarrow \underbrace{\Delta E_{kin}|_{\mu\uparrow}}_{>0} = \underbrace{\Delta E_{for}}_{=0} + \underbrace{\Delta E_{visc}}_{=0} - \underbrace{\Delta E_{int}}_{>0} - \underbrace{\Delta E_{fric}}_{<0} \qquad (2)$$

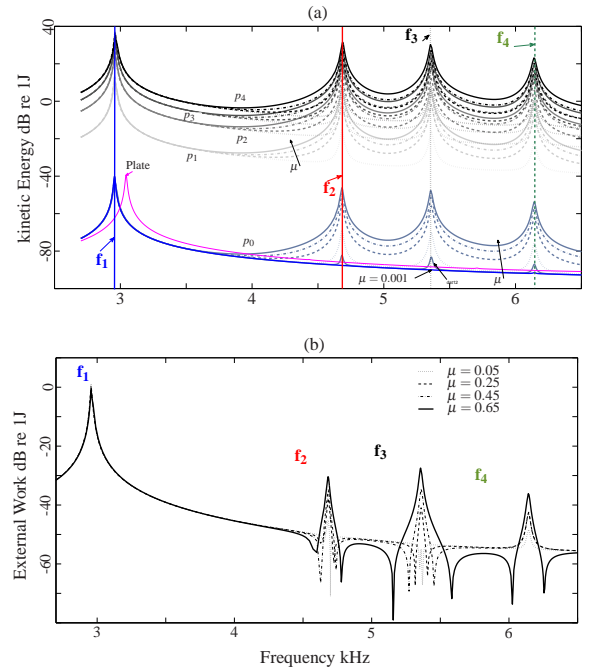Figure 9: (colour online) Standard deviation estimates ($\bar{\sigma}$): (a) Case A - Δ material (ΔM); (b) Case B - Δ load (ΔL); (c) Case C - Δ load and material ($\Delta L + M$),(d) frequency of P_t for Cases A to C and variations $\delta_i \in \{m_i, p_i, MP_i\}$ with $\delta_i, i \in \{1, ..., 4\}$;

Figure 10: (colour online) (a) Kinetic energy for $p_0 = 1\text{kPa}-p_4 = 8.0\text{MPa}$ and $\mu \in \mathscr{M} = \{0.05, 0.25, 0.45, 0.65\}$). f_1-f_4 indicate peaks in the energy spectrum; (b) External work $p = 1\text{kPa}$ and over varying μ

Since a single transfer or point mobility, as performed in [58], only gives the system's response at one point on the structure, a global measure of the amplitude of the vibration level is preferred. The system's kinetic energy $E_{kin} = \int_V \frac{1}{2}\rho \mathbf{v}\mathbf{v}\mathbf{d}\mathbf{V}$ [64] is a measure which accounts for the system's global vibration level and may be used to predict vibrationally very active pad modes. Here V is the volume of the structure, $\mathbf{v}$ the velocity field and ρ the structure's mass den-

Here, E_{for}, E_{visc}, E_{int} and E_{fric} are the energies due to the applied external forces, viscous dissipation, internal forces and friction, respectively. However, no viscous damping is applied here and the external forces are constant. From Figure 10(a) it can clearly be stated, that at most frequencies the kinetic energy increases with increasing p or μ. Therefore, the $\Delta|_{\mu\uparrow}$ in equation (2) stands for changes due to increasing the friction coefficient. As the change in the internal energy is always greater than or equal to zero for an increase in the friction coefficient, the increase in kinetic energy at

some peaks are related to negative frictional work, which is higher, than the increase in strain energy. As the negative external work describes work done by external forces including friction, not available for the internal work, due to friction energy stored in contact springs, the increase in kinetic energy describes the releases fed-in energy at theses frequencies [58, 64, 59].

In Figure 10(b), the external system's work (E_W) is plotted for a range of friction coefficients from 0.05 to 0.65. E_W is composed of frictional energy and work done by the external forces, $E_W = E_{for} + E_{fric}$. As the E_{for}-term remains constant, E_W can only become negative due to the friction term. As negative values are not defined for $\log_{10}$, the logarithm of $|E_W|$ was taken. Evidently, at f_3 which corresponds to pad modes ($4^{th}, 5^{th}$) feeds in most of the energy, then f_4 and f_2 followed by f_1. Peaks of kinetic energy at two frequencies (f_1, f_3) are analysed in detail in Figure 11. For illustrative purposes, the curves were smoothed by means of Hermite interpolation [65] as only five pressures were calculated to obtain the kinetic energy. For this purpose, the peak energies at frequencies f_1 and f_3 are extracted: it can be seen that one is moving on the vertical line in Figure 10(a) from lower to higher pressure values, such representing development of *peak kinetic energy* over (a) pressure or (b) friction coefficients. Also, the logarithm of the identity function $10\log_{10}(p)$ and its square are depicted for reference purpose. Clearly, as the dB values are on a logarithmic
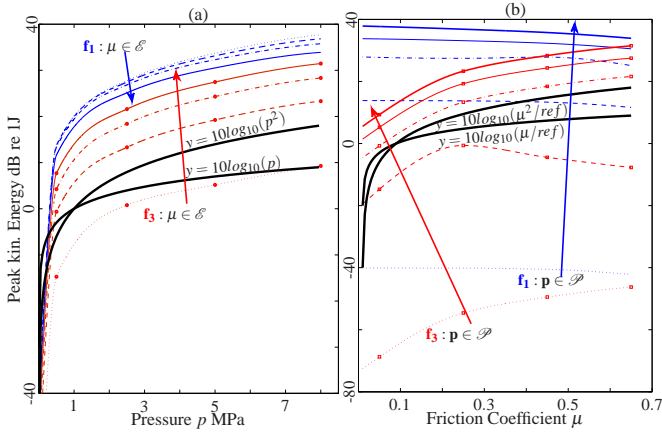

Figure 11: (colour online) Scattering of peak amplitudes of kinetic energy of isotropic pad-on-plate model (I) exemplified for resonances f_1 and f_3 by varying (a) pressure or (b) friction coefficient by leaving either μ or p constant, respectively

scale, increasing the pressure gives an almost quadratic increase in kinetic energy (see $10\log_{10}(p^2)$ for comparison in Figure 11). Further, the behaviour of both familiy of curves, for resonance f_1 and resonance f_3 is consistent, giving the same slope for peak kinetic energy over pressure. However, the two peaks show different behaviours: at f_1, the peak amplitude decreases whereas the second frequency shows a strong increase with greater μ. The behaviour of frequencies f_2 and f_4 in Figure 10(a) is similar to that of f_3 in Figure 11, only less accentuated. As shown in Figure 10(a), as μ changes to higher values, E_{kin} increases at both f_1 and f_3. However, these behaviours are inconsistent, being either linear or non-linear depending on the pressure applied. Also, no clear trend can be found. Based on this, a prediction without calculating directly kinetic energy variations due to friction coefficient changes is more difficult than those due to pressure variations. In Figure 12 the kinetic energy spectrum of the isotropic pad-on-disc model III is depicted. The question is whether the pad modes also exist and whether their effect is similar to that of the pad-on-plate. In order to study the fluctuating character of the modes, the subspace projection method (S) is used to calculate the kinetic energy spectrum for three different Young's moduli $170, 210$ and 249GPa (Figure 12(a)). Of course, for steel, as pressure variations cannot be responsible for such large material property changes, temperature effects,
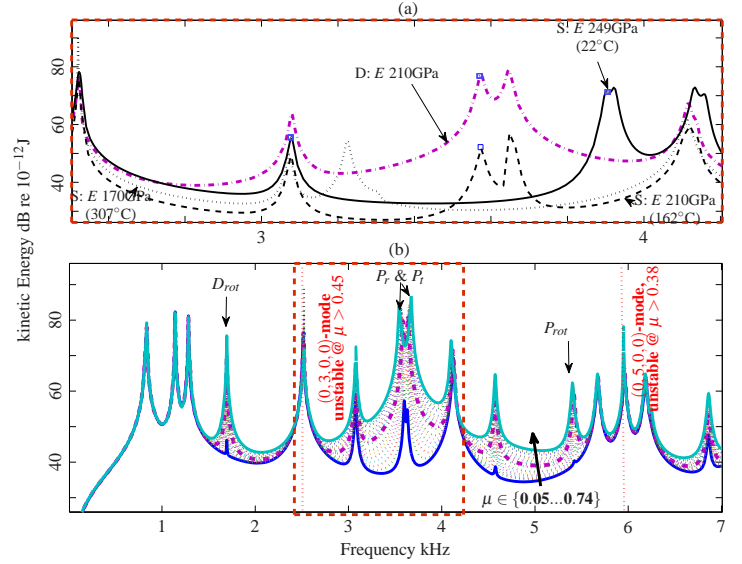

Figure 12: (colour online) Energy spectra of isotropic pad-on-disc model (III): (a) window E_{kin} show fluctuations of pad modes due to elevated temperatures ($E, \nu \pm 18.9\%$) for S - subspace projection method and D - direct steady-state analysis; and (b) kinetic energy spectrum for $E = 210$GPa (Table 1) of D - direct steady-state analysis)

which are more severe, are considered here ($22, 162, 307°C$). The pad modes, which exist for the pad-on-plate model also exist for the pad-on-disc at around $3 - 4$kHz and 5.5kHz. However, the lining does not deform as strongly as depicted in Figure 3(c) and (d) due to steel being the pad material. As a result, due to changes in the Young's modulus (23.5%), variations of frequency in the pad modes (P_r, P_t) are large, around 789Hz or 25.38%, relative to the mode at 170GPa. At $E = 210$GPa, the pad modes lie almost equally apart from the peaks, at around 3.1 and 4.1kHz. Then, for $E = 210$kPa of Young's modulus, the direct steady-state analysis in ABAQUS is used for the friction coefficient from 0.05 to 0.74, to calculate the kinetic energy spectrum, as depicted in Figure 12 (b). The dashed line shows the previously calculated frequency in Figure 12 (a) and $l = 0, P_r, P_t$ and P_{rot} describe an in-plane tangential shear mode and the radial, tangential and rotational pad modes, respectively. Two instabilities are detected by the CEA: the $(0, 5\pm, 0, 0)$ split-mode pair (at $\mu > 0.38$) and the $(0, 3\pm, 0, 0)$ split-mode pair (at $\mu > 0.45$). Obviously, as the friction coefficient increases, the pad mode's change in kinetic energy is dominant and other frequencies at which the spectrum lifts up are clearly visible (e.g., at around 3 or 4.6kHz). At these locations, the qualitative motion of the pad for the animated mode shape is often equal to the motion of one of the pad modes, even though their amplitudes might be very small. D_{rot} describes an in-plane shear mode of the disc at 1.7kHz, which also shows a significant increase in E_{kin}. The dependency of kinetic energy on pressure and friction coefficient is illustrated for 4 modes of the pad-on-disc model in Figure 13. The pressure dependency looks different from that for the pad-on-plate model (Figure 11): the family of curves, although being in the same resonance show changing slopes, which have the tendency of getting flatter for resonances, which decrease with increasing friction (e.g. f_1, f_2) and getting steeper for curves with increasing peak kinetic energy values. However, the general shape remains consistent for all modes and the behaviour can be described as rather *predictable*. The dependency on the friction coefficient is again mainly not predictable: trends in one family of curves change and also different resonances show qualitatively very different behaviour. The identity function $id(p) := p$ and its square are depicted for reference in Figure 13 as well.

As a next step, the global kinetic energy of the an-isotropic pad-on-disc model is analysed with setting $\mu = 0.5$. In Figure 14(a), the ki-

netic energy spectrum for Cases A to C, which were previously analysed by means of the CEA method, is depicted. In Figure 14 for case A, in which only the material properties are varied and the pressure limited to only 1kPa, two peaks, corresponding to P_r and P_t, keep changing their frequencies and amplitudes. The absolute changes

Figure 13: (colour online) Peak kinetic energy (E_{kin}) model III, dependent on (a) p with $\mu = const.$; and (b) μ with $p = const.$; (i) and (iii) frequencies f_1 and f_2, (ii) and (iv) unstable $n = 3$ mode and tangential pad mode P_t

in amplitude of both modes, P_t and P_r, is around 10dB. In Figure 7(b), by increasing the pressure from only 0.5MPa to 8.0MPa (case B), the radial pad mode is pushed out of the frequency band of 3.7-5.0kHz. Only the mode P_t remains visible. Changes in amplitude due to pressure are high up to 0.5MPa above which are not so pronounced and the maximal variations are only around 8dB. Case C in Figure 14(c) shows that for the combined effects of pressure and material properties, (i) the overall vibration level expressed in E_{kin} is higher than for case A and B, (ii) the amplitude is increased by around 3dB from 1kPa to 8MPa; and (iii) the amplitudes of the modes that are not primarily pad modes also increase. In Figure 14(d) the kinetic energy spectrum for various friction coefficients, pressures and material properties is depicted. For $p_0 = 1$kPa the material properties of m_1 were used. Evidently, the kinetic energy of the rotational pad mode P_{rot} is not distinguishable anymore for pressures higher than 0.5Mpa, the same for the radial pad mode P_r. It is worthy to mention, that changes in frequency up to 180Hz can clearly be observed for the tangential pad mode P_t. Also, although the geometry of the structure remains the same, the change from steel to anisotropic lining material reduce the peaks of the energy spectrum by 4 to only at most 11. The kinetic energy for the case of 1kPa uniformly distributed pressure is lower but increases in the end up to 150dB which marks the different behaviour of steel and brake lining behaviour: a steel pad gives an overall higher vibration level at low pressures, than the brake lining, but does at high pressures vibrate on basically the same level . The kinetic energy of the isotropic pad-on-disc system is also around 150dB. In the past, the connection between non-linearity for lower pressures and the occurrence of brake squeal, which often develops at lower pressures [35, 44] and at the beginning of a reduction in a car's speed [27] was mentioned. In [66] radial bursts of the pad's motion were observed while reducing the car's speed. Whether this mechanism is a purely transient process or can also be observed with constant speed due

to some perturbation is yet not fully understood. In any case, the vanishing radial pad-mode visible for the anisotropic pad-on-disc model IV in Figure 14(b) (d) is connected to this phenomenon at low pressures. If the kinetic energy can be related to the acoustic power, then the peak in the spectrum of the in-plane radial pad mode P_r marks an increased likelihood of squeal at lower pressures (here $0.001 - 0.5$MPa) which is a frequenclty encountered phenomenon.

PHASE-SPACE REPRESENTATION OF MECHANISMS INVESTIGATED

In this section, the phase-space plots and calculations of dynamic invariants of the steady-state response of the pad-on-plate model I is presented to show that the system has the tendency to become unstable when the friction coefficient is increased. As mentioned earlier, this instability is not due to the mode-coupling type of instability which would have been detected by the CEA. In the following, only the velocity response at point N in Figure 1(a) is taken. A pressure excitation of 1kPa is linearly swept through the frequency domain. The resolution in the frequency domain for the $N/2$−point transfer function was $\Delta f = 0.5$Hz. The time series was synthesised by applying an inverse Fourier transform to the imaginary surface velocity term. In order to reconstruct the dynamic's phase space, embedding parameters were estimated by means of time-delay embedding using the averaged auto-mutual information and the false nearest neighbour algorithm [67, 68]. With the algorithm of Sano and Sawada [69] the Lyapunov spectrum and as a correlation dimension estimate the Kaplan-Yorke dimension were calculated [70, 71]. In Figure 15, the phase-space representation of the plate's velocity in the x-, y- and z-directions, measured at point N (Figure 1(a)), is depicted. In each subplot, the maximal Lyapunov exponent and the
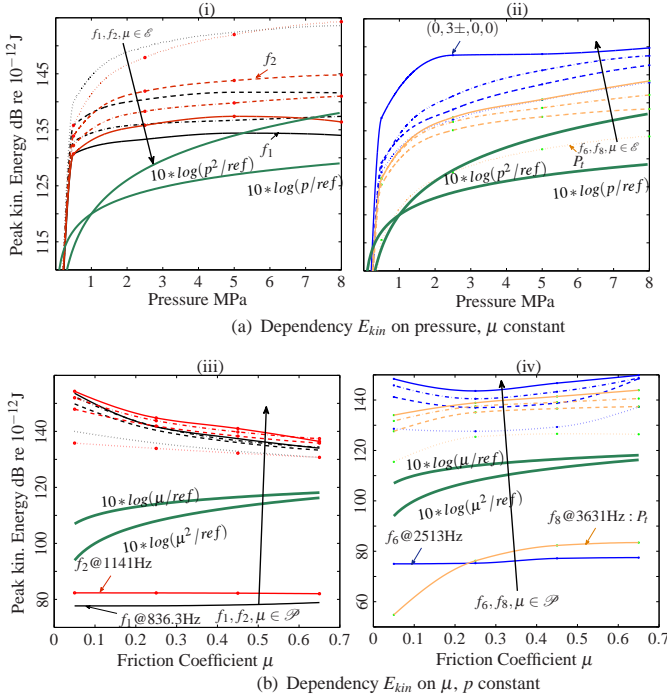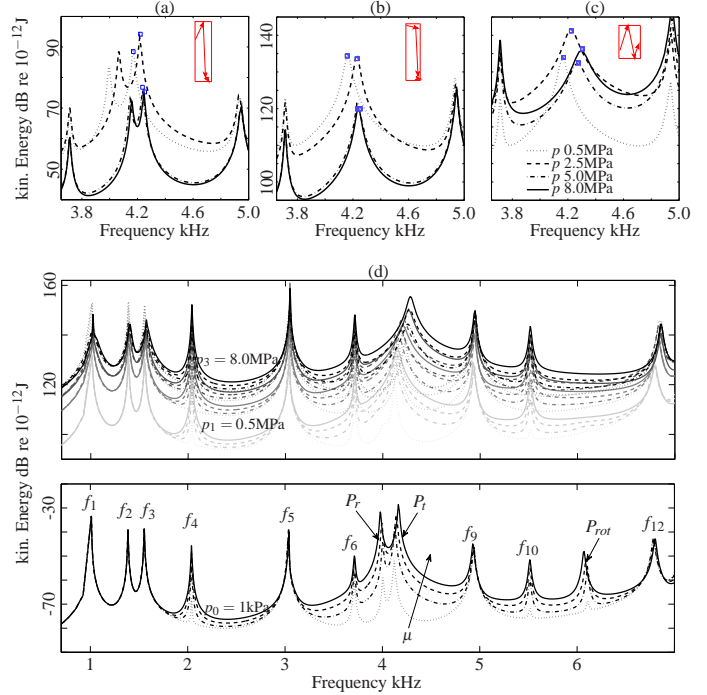

Figure 14: (colour online) Spectra of kinetic energy of model IV for: (a) Case A; (b) Case B; and (c) Case C. The small squares, as fixed points on the peak values, indicate the movement of the frequency peaks; squares with arrows schematise this movement of peaks in a vector plot. (d) Variation of friction coefficient for pressures $p_0 = 1$kPa to $p_4 = 8$MPa.

correlation dimension are estimated. As the friction coefficient increases (up to $\mu = 0.25$), (i) the maximum phase-space dimension becomes larger which is indicative of higher vibration amplitudes; the phase-space dimension increases in continuously in x-direction. In y- and z-direction however, the phase space dimension decreases after $\mu = 0.25$. However, the dynamics get more complicated as can

be seen from the (ii) correlation dimension which increases from 1 to over 3 and the Lyapunov exponents, which become for higher friction coefficients slighlty positive.

DISCUSSION AND CONCLUSION

This paper is focussed on analysing pad-modes by means of the complex eigenvalue analysis and the system's kinetic energy spectrum. By simulating a pad-on-plate model, similar to an experiment performed in [1], pad modes were identified and found to be very efficient in feeding-in energy and highly sensitive to stiffness changes. No instability is detected by means of the complex eigenvalue method, hence classical mode coupling is not present. The plate model's extension to a pad-on-disc model with isotropic pad, shows that these pad modes also exist for annular structures. The fluctuation in frequencies of the pad modes is highly dependent on the material composition of the lining material. An extreme case represents an isotropic pad-on-disc model (III) which has to be modelled with a very fine resolution in the contact zone due to this sensitivity [58]. Special care has to be taken in the modelling of pin-on-disc or beam-on-disc setups which utilise steel lining; also, apart from these models, high-performance pads could show higher rates of fluctuation in frequency as they have higher in-plane stiffness [61]. The modelling of boundary conditions as for instance the friction contact or the pad's constraining nodes as shown in [58] is crucial because the pad modes are responsible for increased energy transfer in the sidebands of their eigenfrequencies. Although for a transversely isotropic lining material, frequency changes are only up to 4% for a pad-on-disc system, the friction and/or temperature at the abutment clips might change the lining's or abutment clip's stiffness and induce a shifted position of the pad modes. Also, wear is an important factor as it changes the elastic lining properties by reducing the puck depth, decreasing the mass and, possibly, increasing the contact zone, depending on whether chamfers are used or not.

Further, it is found by means of the complex eigenvalue analysis, that imperfect merging is not only due to viscous damping but also to frictional damping and higher pressures. This supports the possibility of instabilities with increased system damping as suggested in [17].

As the complex eigenvalue analysis itself is unable to predict instability induced by pad-modes, the kinetic energy is found to be a useful global measure to identify a high structural vibration level. It is found that the dependency of the peak kinetic energy E_{kin} at constant μ on pressure is more predictable than that at constant pressure on μ. It is found that the system's kinetic energy generally increases with increasing pressure and friction coefficient. For the first time, non-linear material property changes due to varying pressure are incorporated into complex eigenvalue calculations. By incorporating variations of pressure and the friction coefficient, the quasi-transient process in analysis of disc brake squeal in the frequency domain can be enhanced: Frequency domain analysis are efficient and can substitute computational expensive time domain models to a certain degree. By applying inverse Fourier transform to the transfer mobility of the pad-on-plate model (I) and conducting non-linear time series analysis, the instability is evidenced by an increasing correlation dimension, an increasing phase space dimension and positive Lyapunov exponents. This result supports the experimental findings of [1] indicating that another mechanism apart from mode coupling is responsible for the squeal encountered in the experiment. For friction coefficients greater than 0.25, the phase space dimension decreases, but the dynamics are more complicated.

It is observed in practice that some squeal occurs repeatedly at the same frequency and that others in the same brake system scatter around a certain frequency. The findings presented here indicate that the often-encountered non-repeatability of brake squeal at some frequencies could be due to the pad modes fluctuating as a consequence of stiffness, temperature and pressure changes. Pad

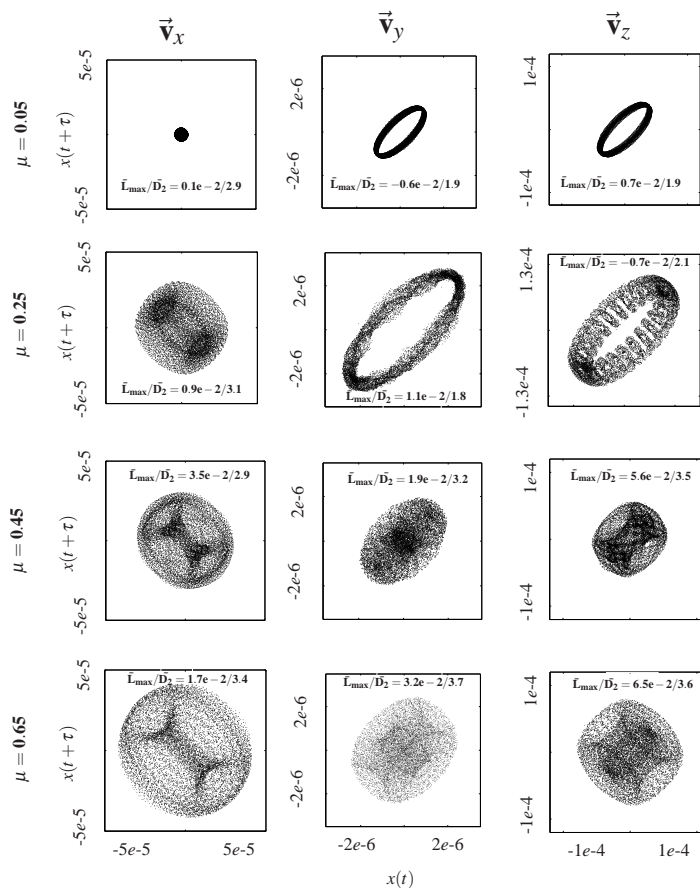modes represent instabilities themselves, and might enhance the

Figure 15: (colour online) Phase-space plots of friction coefficient variations for model I with 1kPa pressure applied. Only plate out-of-plane vibrations at point N (Figure 1) are measured. $\tilde{L}_{max}$, $\tilde{D}_2$ give estimates for the maximal Lyapunov exponent and the correlation dimension respectively.

mode-coupling instability or the efficiency of previously-coupled unstable modes in terms of radiating sound similar to parametric resonances [72, 9]. Initially, the position of these pad modes is dependent on the boundary conditions applied [58]. Therefore, apart from the friction couple as a boundary condition, this is a problem of the designed stiffness and geometry of the abutment clips as well as the bracket design as also investigated in [61].

In the course of a brake application, the lining material changes its stiffness non-linearly. Apart from knowing the composition of the general lining material, its behaviour under dynamic loading is important. Due to increased pressure, compressibility and changed elastic properties, the friction coefficient changes and induces, if increased, additional contact stiffness. It has been shown, that pad modes are sensitive to pressure, material property changes and friction coefficient variations. Significant changes in frequency, due to variations in μ are observed. As in reality the friction coefficient varies a lot, these modes can be called fluctuating, as the strong change in the frequency domain indicates, that in the time domain, their frequency contributes with changing harmonics and strength to the vibration. Due to mesh sensitivity, and a possible amplifying and triggering characteristics of the pad modes, developing a reliable numerical model of a brake system in FEM is a very difficult task. Whether this dynamic instability due to pad modes is truly relevant and efficient in radiating sound is investigated in [73]. A possible solution for assessing the uncertainty of pad-mode instability, caused by variations in frequency, kinetic energy and acoustic power, is presented in [74].

ACKNOWLEDGEMENTS

REFERENCES

[1] F. Chen. Automotive disk brake squeal: an overview. *Int. J. of Vehicle Design*, 51(1/2):39–72, 2009.

[2] F. P. Bowden and L. Leben. Nature of sliding and the analysis of friction. *Nature*, 3572:691–692, 1938.

[3] F. P. Bowden and D. Tabor. Mechanism of metallic friction. *Nature*, 3798:197–199, 1942.

[4] C.M. Mate, G.M. McClelland, R. Erlandsson, and S. Chiang. Atomic-scale friction of a tungsten tip on a graphite surface. *Phys. Rev. Lett.*, 59:1942–1945, 1987.

[5] H.R. Mills. Brake squeak. Technical report, The Institution of Automobile Engineers, Research Report, 9000 B and 9162 B, 1938.

[6] R.T. Spurr. A theory of brake squeal. *Proceedings of the Automobile Division, Institution of Mechanical Engineers 1961-1962 (1)*, 1:33–52, 1961.

[7] M.R. North. Disc brake squeal - a theoretical modell. Technical Report 5, Motor Industry Research Association, Warwickshire, England, 1972.

[8] S.K. Rhee, P.H.S. Tsang, and Y.S. Wang. Friction-induced noise and vibration of disc brakes. *Wear*, 133:39–45, 1989.

[9] J.E. Mottershead, H. Ouyang, M.P. Cartmell, and M.I. Friswell. Parametric resonances in an annular disc with a rotating system of distributed mass and elasticity: And the effects of friction and damping. *Proceedings: Mathematical, Physical and Engineering Sciences*, 453(1956):1–19, 1997.

[10] H. Ouyang, J.E. Mottershead, M.P. Cartmell, and M.I. Friswell. Friction-induced parametric resonances in discs: effect of a negative friction-velocity relationship. *Journal of Sound and Vibration*, 209(2):251–264, 1998.

[11] H. Ouyang. Moving loads and car disc brake squeal. *Noise & Vibration WORLDWIDE*, 34(11):7–15, December 2003.

[12] J.R. Barber. The influence of thermal expansion on the friction and wear process. *Wear*, 10(2):155–159, 1967.

[13] J.R. Barber. Thermoelastic instabilities in the sliding of conforming bodies. *Royal Society of London Proceedings Series A Mathematics Physics and Engineering Science*, 312(1510):381–394, 1969.

[14] G.G. Adams. Self-excited oscillations of two elastic half-spaces sliding with a constant coefficient of friction. *ASME Journal of Applied Mechanics*, 62:867–872, 1995.

[15] G.G. Adams. Steady sliding of two elastic half-spaces with friction reduction due to interface stick-slip. *ASME Journal of Applied Mechanics*, 65:470–475, 1998.

[16] V. Linck, L. Baillet, and Y. Berthier. Modelling the consequences of local kinematics of the first body on friction and on the third body sources in wear. *Wear*, 255:299–308, 2003.

[17] N. Hoffmann and L. Gaul. Effects of damping on mode-coupling instability in friction induced oscillations. *ZAMM, Z. Angew. Math. Mech.*, 83(8):524–534, 2003.

[18] N.M. Kinkaid, O.M. O'Reilly, and P. Papadopoulos. Automotive disc brake squeal. *Journal of Sound and Vibration*, 267:105–166, 2003.

[19] A. Akay. Acoustics of friction. *Journal of the Acoustical Society of America*, 111(4):1525–1548, 2002.

[20] H. Ouyang, W. Nack, Y. Yuan, and F. Chen. Numerical analysis of automotive disc brake squeal: a review. *Int. J. of Vehicle Noise and Vibration*, 1:207–231, 2005.

[21] N. Hoffmann and L. Gaul. Friction induced vibrations of brakes: Research fields and activities. *SAE Technical Paper Series*, 2008-01-2579:1–8, 2008.

[22] S. Oberst, J. C. S. Lai, S. Moore, A. Papinniemi, S. Hamdi, and D. Stanef. Chaos in brake squeal. In *Internoise 2008, Shanghai, 26.-29. October*, 2008.

[23] M.T. Bengisu and A. Akay. Stability of friction-induced vibrations in multi-degree-of-freedom systems. *Journal of Sound and Vibration*, 171:557–570, 1994.

[24] A. Bajer, V. Belsky, and L.J. Zeng. Combining a nonlinear static analysis and complex eigenvalue extraction in brake squeal simulation. *SAE Technical Paper Series*, 2003-01-3349:1–11, 2003.

[25] S. Kung, G. Stelzer, V. Belsky, and A. Bajer. Brake squeal analysis incorporating contact conditions and other nonlinear effects. *SAE Technical Paper Series*, 2003-01-3343:1–11, 2003.

[26] A. Bajer, V. Belsky, and S. Kung. The influence of friction-induced damping and nonlinear effects on brake squeal analysis. *SAE Technical Paper*, 2004-01-2794:1–9, 2004.

[27] N.M. Kinkaid. *On the Nonlinear Dynamics of Disc Brake Squeal*. PhD thesis, University of California at Berkeley, 2004.

[28] A. Felske, G. Hoppe, and H. Matthäi. Oscillations in squealing disc brakes - analysis of vibration modes by holographic interferometry. Technical report, SAE, Technical Report 780333, Warrendale, PA, 1978.

[29] H. Murakami, N. Tsunada, and T. Kitamura. A study concerned with a mechanism of disc brake squeal. *SAE Technical Series*, 841233:1–13, 1984.

[30] F. Chen, S.-E. Chen, and P. Harwood. In-plane mode/friction process & their contribution to disc brake squeal at high frequency. *SAE Technical Paper*, 2000-01-2773:1–15, 2000.

[31] F. Chen, A. Wang, and C. A. Tan. Dynamic system instability suppression with dither technique. In *Proceedings of the 22nd SAE Brake Colloquium, Anaheim, CA*, 2004.

[32] Y. Ichiba and Y. Nagasawa. Experimental study on disc brake squeal. *SAE Technical Paper*, 930802:103–109, 1993.

[33] H. Ouyang, J.E. Mottershead, M.P. Cartmell, and D.J. Brookfield. Friction-induced vibration of an elastic slider on a vibrating disc. *Int. J. of Mechanical Science*, 41:325–336, 1999.

[34] H. Ouyang, J.E. Mottershead, and D.J. Brookfield. A methodology for the determination of dynamic instabilities in a car disc brake. *Int. J. of Vehicle Design*, 23:241–262, 2000.

[35] H. Matsui, H. Murakami, H. Nakanishi, and Y. Tsuda. Analysis of disc brake squeal. *SAE Technical Paper*, 920553:13–24, 1992.

[36] J.-G. Tseng and J. A. Wickert. Nonconservative stability of a friction loaded disk. *ASME Journal of Vibration and Acoustics*, 120:922–929, 1998.

[37] O. Giannini and A. Sestrieri. Predictive model of squeal noise occuring on a laboratory brake. *Journal of Sound and Vibration*, 296:583–601, 2006.

[38] A. Buck. *Simulation von Bremsenquietschen (Brake Squeal)*. PhD thesis, Lehrstuhl für Baumechanik, Technische Universität München, 2008.

[39] J.F. Brunel and P. Dufrenoy. Transient analysis of squealing mode selection in disc brake. *SEA Technical Papers*, 2008-01-2537:1–4, 2008.

[40] G.P. Ostermeyer. On tangential friction induced vibrations in brake systems. *SEA Int. J. Passeng. Cars - Mech. Syst.*, 1(1):1251–1257, 2008.

[41] F. Chen, F. Tan, C./Chen, C. A. Tan, and R. L. Quaglia. *Disc Brake Squeal: Mechanism, Analysis, Evaluation and Reduction/Prevention*. SAE-Society of Automotive Engineers, 2006.

[42] V.P. Sergienko and S. N. Bukharov. Vibration and noise in brake systems of vehicles. part 2: Theoretical investigation techniques. *Journal of Friction and Wear*, 30:216–226, 2009.

[43] D. Yuhas, J. Ding, and S. Vekatesan. Non-linear aspects of friction material elastic constants. *SEA Technical Papers*, 2006-01-3193:1–10, 2006.

[44] G. Lou, L. Lee, and B. Malott. Introduction of anisotropic

lining elastic constants optimisation (alco) method for friction materials. *SEA Technical Papers*, 2007-01-0591:1–8, 2007.

[45] J. Brecht, A. Elvenkemper, J. Betten, U. Navrath, and J.B. Multhoff. Elastic properties of friction materials. *SAE Technical Paper*, 2003-01-3333:1–10, 2003.

[46] E. Wegmann, A. Stenkamp, and A. Dohle. Relation between compressibility and viscoelastic material properties of a brake pad. *SEA Technical Papers*, 2009-01-3017:1–11, 2009.

[47] K. Schiffner, M. Heftrich, and J. Brecht. Modeling of compaction processes of friction material mixes. *SAE Technical Paper*, 2002-01-2594:1–12, 2002.

[48] P. Sanders, T. Dalka, and D. Hartsock. Friction material compressibility as a function of pressure, temperature, and frequency. *SAE Technical Paper*, 2008-01-2574:1–4, 2008.

[49] N. Hinrichs, M. Oestreich, and K. Popp. On the modelling of friction oscillators. *Journal of Sound and Vibration*, 216(3):435–459, 1998.

[50] S. Oberst and J.C.S. Lai. Acoustic response of a simplified brake system by means of the boundary element method. In *NOVEM2009, Keble College, Oxford, England, 5-8April*, 2009.

[51] S. Oberst and J.C.S. Lai. Numerical analysis of a simplified brake system. In *NOVEM2009, Keble College, Oxford, England,5-8April*, 2009.

[52] S. Oberst and J.C.S. Lai. Non-linear analysis of brake squeal. In *ICSV16, Krakow, 5-9 July*, 2009.

[53] S. Oberst and J.C.S. Lai. Numerical prediction of brake squeal propensity using acoustic power calculation. In *Proceedings of ACOUSTICS 2009*, 2009.

[54] J.D. Fieldhouse and T.P. Newcomp. Double pulsed holography used to investigate noisy brakes. *Optics and Lasers in Engineering*, 25(6):455–494, 1996.

[55] A. Akay, F. Giannini, F. Massi, and A. Sestieri. Disc brake squeal characterization through simplified test rigs. *Mechanical Systems and Signal Processing*, 23:2590–2607, 2009.

[56] N.H. Fletcher and T.D. Rossing. *The physics of musical instruments*. Springer-Verlag New York, 1998.

[57] H. Lee and R. Singh. Self and mutual radiation from flexural and radial modes of a thick annular disc. *Journal of Sound and Vibration*, 286:1032–1040, 2005.

[58] S Oberst and J.C.S. Lai. Evaluation of numerical methods for simulating brake squeal noise. In *20th International Congress on Acoustics (ICA 2010) in Sydney, 23 - 27 August, Australia*, 2010.

[59] Dassault Systemes. *ABAQUS/CAE User's MANUAL*, 2007.

[60] J. Chen and B. Young. Stress-strain curves for stainless steel at elevated temperatures. *Engineering Structures*, 28:229–239, 2006.

[61] D. Guan and J. Huang. The method of feed-in energy on disc brake squeal. *Journal of Sound and Vibration*, 261:297–307, 2003.

[62] B. Breuer and K.-H. H. Bill. *Bremsenhandbuch: Grundlagen, Komponenten, Systeme, Fahrdynamik*. Viehweg Verlag, 2006.

[63] D.J. Ewins. *Modal Testing: theory, practice and application*. Research Studies Press, 2000.

[64] *ABAQUS 6.7-1, Theory Manual*.

[65] The MathWorks. *MatLab R2007A*.

[66] N.M. Kinkaid, O.M. OŠReilly, and P. Papadopoulos. On the transient dynamics of a multi-degree-of-freedom friction oscillator: a new mechanism for disc brake noise. *Journal of Sound and Vibration*, 287:901–917, 2005.

[67] N. Marwan, M.H. Trauth, M. Vuille, and J. Kurths. Comparing modern and pleistocene enso-like influences in nw argentina using nonlinear time series analysis methods. *Climate Dynamics*, 21:317–326, 2003.

[68] H. Kantz and T. Schreiber. *Nonlinear time series analysis*. Cambridge University Press, 2004.

[69] M. Sano and Y. Sawada. Measurement of the lyapunov spectrum from a chaotic time series. *Phys. Rev. Lett.*, 55(10):1082–1085, Sep 1985.

[70] R. Hegger, H. Kantz, and T. Schreiber. Practical implementation of nonlinear time series methods: The [small-caps tisean] package. *Chaos: An Interdisciplinary Journal of Nonlinear Science*, 9(2):413–435, 1999.

[71] *Time Series Analysis (TISEAN); http : //www.mpipks − dresden.mpg.de/ tisean/Tisean₃.0.1/index.html*.

[72] Y.S. Kachanov. On the resonant nature of the breakdown of a laminar boundary layer. *Journal of Fluid Mechanics*, 184:43–74, 1987.

[73] S Oberst and J.C.S. Lai. Acoustic radiation due to friction-induced pad mode instability in disc brake squeal. In *20th International Congress on Acoustics (ICA 2010) in Sydney, 23 - 27 August, Australia*, 2010.

[74] S Oberst and J.C.S. Lai. Uncertainty modelling in detecting friction-induced pad mode instabilities in disc brake squeal. In *20th International Congress on Acoustics (ICA 2010) in Sydney, 23 - 27 August, Australia*, 2010.